ACS Photonics

Article

Cite This: ACS Photonics 2018, 5, 3064−3072

pubs.acs.org/journal/apchd5

Shaping Polaritons to Reshape Selection Rules

Francisco Machado,*[,†,‡,⊥] Nicholas Rivera,[‡,⊥] Hrvoje Buljan,[§] Marin Soljačić,[‡] and Ido Kaminer[‡,∥]

[†]Department of Physics, University of California, Berkeley, California 94720, United States

[‡]Department of Physics, Massachusetts Institute of Technology, Cambridge, Massachusetts 02139, United States

[§]Department of Physics, University of Zagreb, Zagreb 10000, Croatia

[∥]Department of Electrical Engineering, Technion, Israel Institute of Technology, Haifa 32000, Israel

Supporting Information

ABSTRACT: The discovery of orbital angular momentum (OAM) in light established a new degree of freedom by which to control not only its flow but also its interaction with matter. Here, we show that by shaping extremely subwavelength polariton modes, for example by imbuing plasmon and phonon polaritons with OAM, we engineer which transitions are allowed or forbidden in electronic systems such as atoms, molecules, and artificial atoms. Crucial to the feasibility of these engineered selection rules is the access to conventionally forbidden transitions afforded by subwavelength polaritons. We also find that the position of the absorbing atom provides a surprisingly rich parameter for controlling which absorption processes dominate over others. Additional tunability can be achieved by altering the polaritonic properties of the substrate, for example by tuning the carrier density in graphene, potentially enabling electronic control over selection rules. Our findings are best suited to OAM-carrying polaritonic modes that can be created in graphene, monolayer conductors, thin metallic films, and thin films of polar dielectrics such as boron nitride. By building on these findings we foresee the complete engineering of spectroscopic selection rules through the many degrees of freedom in the shape of optical fields.

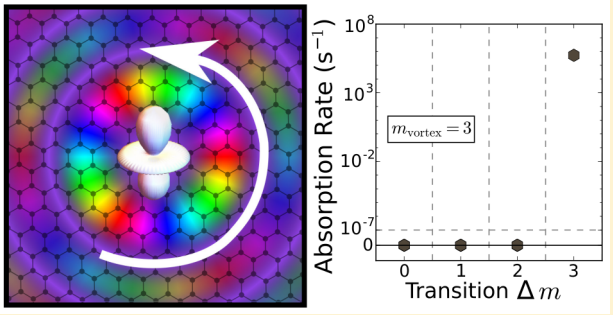

KEYWORDS: *spectroscopy, light−matter interaction, orbital angular momentum, 2D materials, graphene*

The discovery that light can possess orbital angular momentum (OAM)[1] besides its intrinsic spin value of $\hbar$ has brought forth a new degree of freedom for the photon. By engineering the shape of optical modes, a wide variety of new applications has been developed including angular manipulation of objects,[2] angular velocity measurement,[3] higher bandwidth communication using novel multiplexing techniques[4,5] (already with on-chip implementations[6]), quantum information systems,[7] quantum memory,[8] and sources of entangled light,[9] which are beneficial to quantum cryptography implementations.[10,11]

These results open the door for another important application of shaped optical modes: tailoring the interactions between electrons and photons by enhancing or suppressing electronic transitions. For example, when imbuing an optical mode with OAM, one expects novel selection rules based on conservation of angular momentum. This would provide a rich new degree of freedom for spectroscopy and many other studies where optical excitation is relied on for studying and controlling matter. Unfortunately, such control over electronic transitions is not expected to be experimentally accessible because "the effective cross section of the atom is extremely small [compared to the wavelength of light]; so the helical phase front [of an OAM-carrying beam of light] is locally indistinguishable from an inclined plane wave".[12] In other words, the length scale mismatch between the electronic and photonic modes leads to a very small interaction that is beyond what can be observed in most experiments. Such a prediction has been corroborated in several theoretical studies[13−16] and is now taken as a basic fact.[17] This length scale mismatch between the electron and photon makes the relevant transitions so slow that they are considered "forbidden". It follows that in order to achieve control over transitions with OAM, one needs first to find a way to access these forbidden transitions.

It has been shown that it is possible to controllably transfer angular momentum of up to $2\hbar$ in systems of cold trapped ions,[18] where the trapping ensures sufficient interaction time to enable transitions despite the length scale mismatch. However, new approaches may be necessary to extend these ideas to transitions that are much slower, such as higher-order multipolar transitions and also multiphoton transitions. In such an approach, it is absolutely necessary to bridge the disparate length scales of the electronic system and photon.

Recent discoveries in polariton physics, ranging from surface plasmon polaritons (SPPs) in graphene,[19−22] to surface phonon polaritons (SPhPs) in polar dielectric films,[23−25] may provide the answer as a result of their extremely short wavelengths,

Received: March 13, 2018
Published: July 10, 2018

DOI: 10.1021/acsphotonics.8b00325
ACS Photonics 2018, 5, 3064−3072

predicted to potentially be as small as just a few nanometers. For example, plasmon and phonon polaritons found in materials such as graphene,[19−22,26−28] monolayer silver,[29] beryllium,[30] silicon carbide,[31] and hexagonal boron nitride (hBN)[32−34] can have wavelengths 100−350 times shorter than the wavelength of a far-field photon at the same frequency.

Confining light with either the above materials or nanostructured conventional plasmonic materials is known to strongly enhance the strength of light−matter interactions with nearby emitters and hence the spontaneous emission rates of nearby dipoles.[35,36] Several recent studies have also shown that conventionally forbidden transitions such as quadrupole transitions could be greatly enhanced using highly confined plasmonic fields in nanostructured geometries such as nanoparticles,[37−41] nanoparticle arrays,[42,43], nanowires[44,45] and quantum wells.[46] It was then shown that via the extreme confinement of light in 2D plasmonic and phonon-polaritonic materials, an even greater range of interactions, such as extremely high-order multipolar emission, multiphoton spontaneous emission, and spin-flip emission could become fast or even dominant compared to typically allowed transitions in many atomic emitters.[47,48]

Despite these many studies, no previous work has demonstrated the possibility of *deterministically engineering the spatial profile of a polaritonic mode to subsequently engineer which electronic transitions do or do not happen*. For example, could one imprint OAM onto a plasmonic mode in order to turn on an electronic transition consistent with that OAM or to turn off a transition inconsistent with that OAM? More generally, could one apply this concept to more complex electronic states with less symmetry by matching the shape of the optical field to that of the electronic orbital, strongly enhancing (or suppressing) emission or absorption?

In this paper we show that by shaping the polaritonic modes of a system we raise the possibility of tailoring the selection rules for absorption and stimulated emission, using OAM-carrying modes as an example. We show that these modes enable new selection rules based on the conservation of angular momentum, providing a new scheme for the efficient control of electronic transitions in atomic systems. We can use OAM-carrying polaritons to allow conventionally forbidden transitions to be fast and dominant, and we can use OAM-carrying polaritons to forbid conventionally allowed transitions. We further find that tuning the placement of the absorber and the dispersion of the polaritons provides a means to study many different electronic processes in a controllable way. Our results are applicable to not only OAM-carrying light but also any form of optical field shaping. Thus, the scheme we propose in this work may open the door to controlling electronic selection rules with the immense number of degrees of freedom in general shaped optical fields. In the long run, combining this technique with ultrafast pulse technology can provide precise spatiotemporal control over the electronic degrees of freedom in myriad systems.

RESULTS

We start our analysis by considering the simplest scenario: an atom placed inside an OAM-carrying polariton mode such that the atom is concentric with the mode's center. This is illustrated schematically in the top left of Figure 1. Taking advantage of recent experimental results showing the ability to generate highly confined vortex polaritons,[49−52] we assume one can generate such modes and focus on the study of their interaction with an atom-like system. For concreteness we consider the atomic system to be hydrogen. Although we use hydrogen as a particular example, the physics we demonstrate in this work can be readily extended to many other atomic and molecular systems, particularly those with spherical or axial symmetry. The OAM-carrying polariton mode, typically called a vortex or vortex mode, can be constructed from the superposition of incoming plane wave polaritonic modes whose phase difference is proportional to the incoming angle as

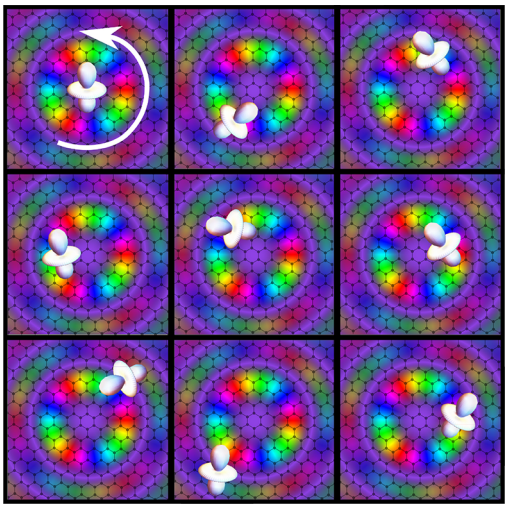

Figure 1. Illustration of a polaritonic vortex and its interaction with an atomic system. An electronic system, such as an atom (in white), is placed near the center of an OAM-carrying polaritonic vortex mode (pictured with OAM = $3\hbar$), exciting transitions consistent with selection rules based on conservation of angular momentum. The strength and phase of the z-component of the electric field of the vortex mode are represented by the color's opacity and hue, respectively. The dark purple background corresponds to the substrate that hosts the vortex mode. By generating many parallel OAM-carrying polaritonic modes one can enhance the resulting signal.

$$\boldsymbol{E}_{q,m}(\boldsymbol{\rho}, z) = E_0 \int_0^{2\pi} \frac{d\alpha}{2\pi} e^{i(q\rho\cos(\phi-\alpha)-\omega t)} \frac{\hat{q} + i\hat{z}}{\sqrt{2}} e^{-qz} e^{i\alpha m}$$
$$\Rightarrow E_z \propto J_m(q\rho) e^{im\phi} e^{-qz} \quad (z > 0) \tag{1}$$

where $\boldsymbol{E}_{q,m}(\boldsymbol{\rho}, z)$ is the electric field profile of the mode, J_m is the Bessel function of order m, $\boldsymbol{\rho} = \{\rho, \phi\}$ are the in-plane distance and angle, z and $\hat{z}$ are the out-of-plane position and direction respectively, α is the angle of the incoming plane wave polariton in direction $\hat{q}$, q its wavenumber, ω its angular frequency, and E_0 its amplitude.

The most important parameters in our analysis are the confinement factor of the vortex and its OAM. The confinement factor η measures how small the wavelength of the mode is relative to the wavelength of a free space photon of the same frequency and is defined by $\eta = qc/\omega$. The OAM of the mode is given by $\hbar m$ where m is the phase winding of the vortex. For example, in Figure 1, we show the phase profile of vortex modes with an OAM of $3\hbar$. Throughout the text, we assume that the polariton vortex is created in a 2D plasmonic material with Drude dispersion. We arrive at quantitatively similar results for finite thickness substrates and other dispersion relations, such as those of phonon polaritons, provided that the confinement factors are the same. This is explained in detail in the Supporting Information (SI).

DOI: 10.1021/acsphotonics.8b00325
ACS Photonics 2018, 5, 3064−3072

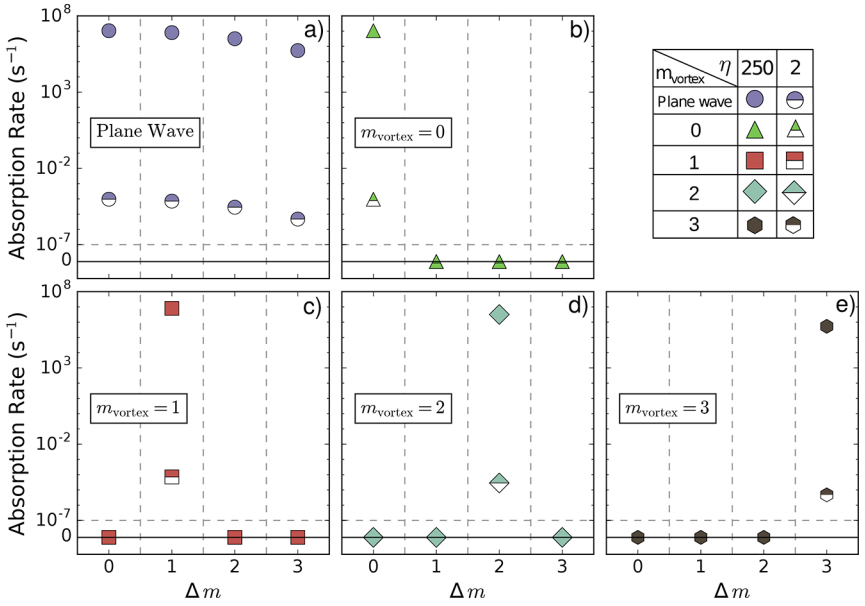

Figure 2. Selection rules in the absorption of OAM-carrying SP(h)P modes. Calculation of the absorption rate due to a plane wave SP(h)P (a) and an OAM-carrying vortex SP(h)P (b−e) for different transitions in the family (5, 0, 0) → (6, 3, Δm) for two different values of confinement factor η, 2 (half-filled) and 250 (filled), with the atom taken to be 20 nm away from the surface. The vortex modes impose selection rules on the electronic transitions, while the increase in confinement factor leads to an enhancement of the absorption rate by a factor of $\sim 10^{11}$. The examples of $\eta = 2$ show that, although free-space OAM-carrying modes could in principle impose the same selection rules, the difference in length scales between the polariton and the atom results in absorption rates too small for experimental observation. The absorption rates are normalized by assuming each SP(h)P mode carries a single photon.

In Figure 2, we consider the effect of the vortex polariton modes on the absorption rates of different transitions, calculated to first order in perturbation theory. For concreteness, we consider a set of transitions between principal quantum numbers 5 and 6 (with a transition free-space wavelength of 7.45 μm). In the example explored in this figure, we consider the octupole (E3) transition between the 5s state and the $6f_{0,1,2,3}$ states. Normally such a transition is considered highly forbidden. The atom is taken to be 20 nm away from the surface of the polariton-sustaining material. In principle, the hydrogenic states can be nonperturbatively modified as a result of the van der Waals force between the atom and the plane of the polaritonic material. The energies of the states will be modified on the order of 0.1−0.001 meV[33] for an atom 20 nm away from the surface of a conductor, and the wave functions can be mixed. However, even if this happens, the cylindrical symmetry of the hydrogenic states is not modified and the transitions follow the selection rules that we arrive at in eq 2. Transitions differing by orbital angular momentum greater than $\hbar$ will still be forbidden within the dipole approximation. As a result, we ignore these complications in this work and use the bare hydrogenic states as well as their bare energies. In Figure 2(a), we consider the absorption rate of a plane wave polaritonic mode and observe that transition rates between different Δm states are all nonzero. All transitions are allowed, and there is no control over the electronic dynamics. In contrast, when considering the absorption of a vortex mode with m_{vortex} = 0, 1, 2, 3 in Figure 2(b−e), respectively, only the transition corresponding to conservation of angular momentum is nonzero, the remaining transitions have been suppressed.

These selection rules arise naturally in the Fermi's golden rule formalism in a cylindrically symmetric system. In this case the transition rate is proportional to the square of $\int_0^{2\pi} d\phi\ e^{-i(m_f - m_i)\phi} e^{im_{vortex}\phi}$, where $\hbar m_i$ and $\hbar m_f$ are the z-projected angular momentum of the initial and final electron states and m_{vortex} is the phase-winding index of the polariton vortex mode. This proportionality makes it clear that the transition rate is zero unless

$$\Delta m = m_f - m_i = m_{vortex} \quad (2)$$

This simple equation tells us that differences in the z-projected OAM of the electron must be supplied by the vortex, thus justifying the interpretation of the phase winding as an angular momentum. The reason that plane waves do not yield the same level of control is that a plane wave is equivalent to a superposition of vortices with all possible angular momenta. Therefore, the angular momentum selection rule is always satisfied for some transition where an electron absorbs a plane wave. The result of eq 2 relies only on axial symmetry of the potential that the electron experiences. As a result, the selection rules of eq 2 are robust to perturbations such as those induced by van der Waals forces between the emitter and the planar dielectric slab.

Although eq 2 tells us which transitions are allowed and which are not, it does not tell us in advance if the allowed transitions happen quickly enough to be observable. To this end, in Figure 2, we also quantify the rates of different electronic transitions due to the absorption of unshaped (plane wave) polaritons, as in Figure 2(a), and shaped (vortex) polaritons, as in Figure 2(b−e). In all cases in this work, we take the intensity of the driving field at the transition frequency to be that associated with a single polariton (for more details see SI Section III). In both cases, the absorption rates are a sharp function of confinement. For a confinement factor of 2, the nonzero E3 transitions rates are on the order of 1 event per 10 hours, while at a confinement of 250, the rates are on the order of 1 event per 300 ns (for an atom 20 nm away from the material's surface), an 11 order of magnitude enhancement. As the atom gets even closer to the surface (for example when the atom is 5 nm away), the rate can

DOI: 10.1021/acsphotonics.8b00325
ACS Photonics 2018, 5, 3064−3072

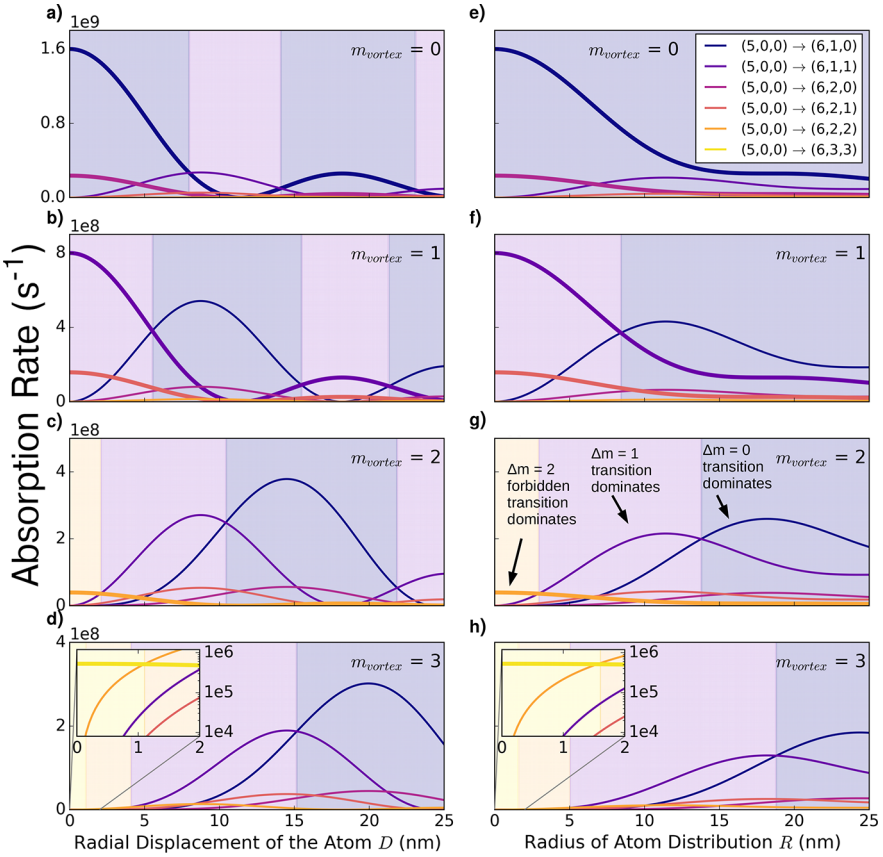

Figure 3. Robustness of the angular momentum selection rules to atom displacement. Dependence of the single polariton absorption rates of a displaced individual atom (left column) and uniform atomic distribution (right column) for transitions with initial state (5, 0, 0) and final principal quantum number 6 at a confinement factor of $\eta = 250$ and the atom taken to be 20 nm away from the surface. As the rotational symmetry is broken, the selection rule discussed in Figure 2 is no longer valid and all Δm transitions become allowed. The absorption rates match the selection rule of eq 2 at $D = 0$, and for small D this transition always dominates. For larger D, other transitions can become dominant, as the value of $J_0(qD)$ decreases and higher order Bessel terms become comparable. The background color of each plot corresponds to the dominant transition in that regime. The angular-momentum-conserving transitions are highlighted by a thicker line.

increase to nearly 1 event per 500 ps, which would be considered fast even for (free-space) dipole transitions. These quantitative results make it evident that angular momentum conservation alone is insufficient to ensure experimentally accessible selection rule modification: it is also imperative to match the scale of the atom and photon.

A notable consequence of the results presented in Figure 2 is that using SP(h)P vortex modes yields *highly enhanced and controllable* electronic transitions for arbitrarily large values of Δm, in contrast to the case with plane wave (unshaped) polariton modes. In particular, by creating a vortex with a fixed OAM and placing atoms concentric with that vortex, it is possible to forbid conventionally allowed dipole transitions (by making the OAM of the vortex greater than 1) and allow conventionally forbidden multipole transitions, thus providing a way to access and control conventionally disallowed transitions which are normally invisible in spectroscopy.

Before proceeding to further analyze the ability to control electronic transitions with shaped optical modes, we pause to discuss some experimental considerations in implementing the above results. Schematically, an experiment to observe the effects described in this paper would feature a polariton-sustaining surface, absorbing atoms, and a means to create vortex modes with different angular momenta in the vicinity of these atoms. The goal is to observe the modified absorption of the sample as a function of the angular momentum of the vortex, which can be indirectly probed by monitoring the fluorescence of the sample as a result of its interaction with the vortex. An important requirement of the polariton-sustaining surface is that its wavelength is comparable to the size of the orbitals of the atoms. Because of that, optimal materials for creating vortices include ultrathin films of plasmonic (gold, silver) or phononic (silicon carbide, boron nitride) materials or 2D conductors such as graphene. Creating the vortices can be done by illuminating an appropriately shaped grating coupler near the surface.[49−52] Of course, the radius of the coupler should be comparable to the polariton wavelength so that the polariton does not decay completely when propagating to the center. We assume this situation throughout the text. Finally, we note that while polaritonic vortices have been demonstrated in plasmonic materials such as gold and silver, they have yet to be demonstrated in graphene or phonon−polariton materials. Therefore, a first and exciting step toward implementing our proposed scheme is to generate vortices in these materials.

Regarding the choice of absorbing atom, because the results of Figure 2 are for an atom centered with the vortex, our scheme is most cleanly implemented on atom-like systems whose placement can be controlled very well, such as quantum dots. Another potential advantage of quantum dots is that they can be made to have mesoscopic sizes, allowing one to match the length scales of the vortex with the size of the atom-like system more easily (i.e., a smaller polariton confinement is required). For

DOI: 10.1021/acsphotonics.8b00325
ACS Photonics 2018, 5, 3064−3072

example, for a practicable quantum dot size of 20 nm,[54] one should be able to access and control conventionally forbidden transitions through the use of vortices of 70 nm wavelength, which have already been demonstrated on thin silver films.[49] For even larger quantum dot sizes, it is conceivable that the same effects we describe here could be observed by using vortices of conventional surface plasmons even on thick metallic films.

However, while the scheme we propose can be more readily implemented with artificial atoms, it would be of appreciable interest to implement it with the much smaller natural atomic and molecular systems, whose myriad forbidden multipolar transitions have been elusive to spectroscopy since its early days. And while it is potentially possible to find polaritons that are sufficiently highly confined to be interfaced with atomic and molecular emitters,[47] a challenge in implementing our scheme arises from the considerable uncertainty in the placement of the atom. Therefore, we now study the effect of off-center displacement of the atom on the prospects for access and control over forbidden transitions.

When an atom is off-center from the vortex, as illustrated in Figure 1, the rotational symmetry around the vortex center is broken, meaning that angular momentum conservation no longer holds. More explicitly, the absorption rate of a vortex by an off-center atom is no longer related to $\int_0^{2\pi} \mathrm{d}\phi\ \mathrm{e}^{-i(m_f - m_i)\phi}\mathrm{e}^{im_{\mathrm{vortex}}\phi}$ but rather

$$\int_0^{2\pi} \mathrm{d}\phi\ \mathrm{e}^{-i(m_f - m_i)\phi} \sum_{m=-\infty}^{\infty} C_{m-m_{\mathrm{vortex}}}^{\phi_0} \mathrm{e}^{\mathrm{im}\phi} J_{m-m_{\mathrm{vortex}}}(qD)$$

where q is the wavenumber of the polariton vortex mode, D is the radial separation between the atomic and the vortex center, and $C_{\delta m}^{\phi_0}$ is a complex number of unit magnitude ($|C_{\delta m}^{\phi_0}| = 1$) dependent on $\delta m = m - m_{\mathrm{vortex}}$ and the angular position of the atom ϕ_0. The full derivation can be found in the SI. As a result, the rate of absorption of a single polariton vortex (of angular momentum $\hbar m_{\mathrm{vortex}}$) at a distance D for a transition between states i and f with a change in the z-projected angular momentum $\hbar\Delta m$, denoted $\Gamma_{m_{\mathrm{vortex}}}(\mathrm{i} \to \mathrm{f}, D)$, becomes

$$\Gamma_{m_{\mathrm{vortex}}}(\mathrm{i} \to \mathrm{f}, D) = J^2_{\Delta m - m_{\mathrm{vortex}}}(qD)\Gamma_{\Delta m}(\mathrm{i} \to \mathrm{f}, 0) \quad (3)$$

where $\Gamma_{\Delta m}(\mathrm{i} \to \mathrm{f}, 0)$ is the rate of absorption of a single vortex polariton when the atom is aligned with the vortex mode of OAM $\hbar\Delta m$. Note that for $D = 0$ (centered atom) the rate is only nonzero when the transition satisfies $\Delta m = m_{\mathrm{vortex}}$, in agreement with eq 2. Eq 3 is physically consistent with an analogous result that has been obtained in the context of the absorption of far-field twisted light by atomic systems.[55]

Eq 3, while a rather simple result, contains much interesting physics, which Figures 3 and 4 intend to summarize. The most obvious consequence of eq 3 is that when the atom is off-center relative to the vortex ($D \neq 0$), the nonzero value of the Bessel function, $J_{\Delta m - m_{\mathrm{vortex}}}(qD)$, allows for transitions that were forbidden when $D = 0$. Since the argument of the Bessel function in eq 3 is qD, the strength of the different absorption processes varies at the length scale of the wavelength of the vortex mode and not the size of the atom. This means that the interaction is robust to misalignments of nanometers or even tens of nanometers and is not sensitive to fluctuations on the atomic scale. For the remainder of this section, we shall refer to the originally allowed transitions for $D = 0$ as angular-momentum-conserving, and the originally disallowed ones as non-angular-momentum-conserving.

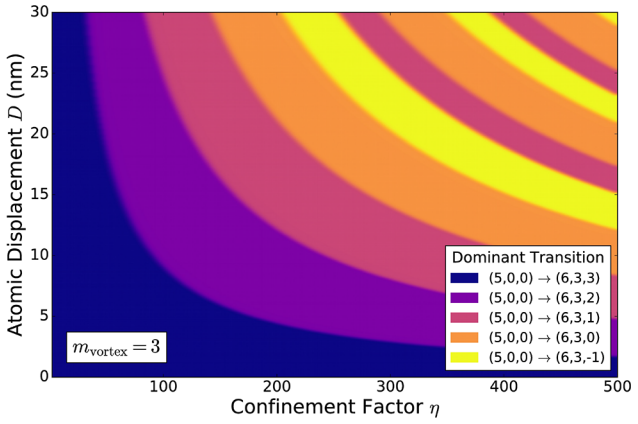

Figure 4. Landscape of dominant transitions for $m_{\mathrm{vortex}} = 3$. For a hydrogen atom taken to be 20 nm away from the surface, the dominant process in the family $(5, 0, 0) \to (6, 3, \Delta m)$ is plotted as a function of the confinement factor η and the displacement of the atomic system D. For a given vortex mode, the displacement and confinement can be used to control the dynamics of the electronic system. This is of particular interest in materials such as graphene, where the confinement factor of the mode can be electrically tuned, opening the possibility for electrical control over atomic transitions.

In Figure 3(a–d), we calculate the rates of different absorption transitions between initial state 5s and final states with principal quantum number 6 as a function of atomic displacement D for varying vortex OAM (increasing from top to bottom). For zero radial displacement, only angular-momentum-conserving transitions (highlighted by a thicker line) have a nonzero absorption rate, as dictated by eq 2. As the radial displacement of the atom is increased, the rate of non-angular-momentum-conserving transitions increases and eventually may dominate over angular-momentum-conserving transitions. Although this appears to reduce control over electronic transitions, because of the oscillatory behavior of the Bessel function with displacement, there are regimes where one particular transition (though not necessarily the angular-momentum-conserving one) dominates over all others, providing a parameter to tune which transition dominates. These regimes in Figure 3(a–d) are marked using the colored background, where the colors denote which transitions dominate. Additionally, a single vortex can be used to "turn off" certain absorption transitions because the absorption rate has nodes where the Bessel function vanishes, as can also be seen in Figure 3(a–d). This means that, somewhat surprisingly, a *single vortex* can actually be used to controllably (through D) access and study different transitions, beyond what angular momentum conservation dictates. We conclude the analysis of Figure 3(a–d) by pointing out that this controlled access is yet again possible only because the rates of transitions calculated in these figures are sufficiently high that these transitions can be observed. Were the confinement factor 2, the transitions would be 11 orders of magnitude slower, and this degree of control using atomic placement would be rendered inaccessible.

The analysis presented in Figure 3(a–d) is pertinent to the case when a single atom is placed exactly at a radial displacement D from the center of the vortex, which is expected to well-characterize a mesoscopic absorber with a more precise placement, such as a quantum dot. In Figure 3(e–h), we consider the case where a population of randomly distributed absorbing atoms interacts with the polariton vortex. In these panels, the average rate of absorption of the sample is computed

DOI: 10.1021/acsphotonics.8b00325
ACS Photonics 2018, 5, 3064–3072

as a function of vortex angular momentum and the radius R of the random uniform distribution of atoms, which experimentally might be set by the deposition conditions. The effect of the distribution is to average the results of Figure 3(a–d) over D. Despite this averaging, R can still be used as a reliable parameter for tuning the dominant transition in the system, as highlighted in the changing colored backgrounds in Figure 3(f–h). Therefore, it still is the case that the radius of the distribution/sample size can be used to make non-angular-momentum-conserving transitions dominant, thus acting as a parameter to control the strengths of different once-forbidden transitions.

In Figure 3, we have discussed the effect of the radial displacement D, but eq 3 tells us that the wavenumber of the vortex mode serves equally well as a tuning parameter by which to control which transitions dominate and which ones do not. In polaritonic platforms such as graphene, it is already possible to tune the wavenumber of the plasmon at a fixed frequency by changing the carrier concentration (or equivalently Fermi energy, E_F). The wavenumber depends on the doping level in graphene via $q = \frac{2\alpha\omega}{\bar{\epsilon}_r c}\frac{\hbar\omega}{E_F}$, where $\bar{\epsilon}_r$ is the average dielectric constant surrounding the film[19,28] and α is the fine-structure constant. This formula is correct within the Drude model formalism with some correction typically at larger values of q. In Figure 4, we explore the consequences of tuning the polariton wavenumber on controlling forbidden electronic transitions. We consider the absorption rate of a polariton vortex (for a fixed OAM of $3\hbar$) for different transitions ($5s \rightarrow 6f_{\Delta m}$) as a function of the radial displacement D and the confinement factor $\eta = qc/\omega$, which directly modifies the wavenumber q. The colored regions indicate which transition of this family dominates. As can be seen, for fixed radial displacement, as the confinement (or Fermi energy) is tuned, we can choose which transition dominates. In fact, at a radial displacement of 30 nm, we can switch between five different transitions by tuning the confinement factor between 1 and 250. Analogous to Figure 3(e–h), when considering a uniform distribution of absorbers, the radius of this distribution still provides a good parameter for controlling the dominant transition, as illustrated in the SI. More detailed information regarding the rates of these different transitions can also be found in the SI.

Before concluding we note that in order to tune the confinement factor while keeping the same vortex OAM, one would need a near-field coupling scheme such as a circular grating where the phase of the emission at different points in the grating is set so that the phase winds m_{vortex} times, irrespectively of the confinement factor. This ensures that the relative phases of the in-coupled (plane wave) polaritons are fixed as we vary the confinement factor of the mode, thus retaining the necessary interference to build the vortex. One way to potentially achieve this is by illuminating a circular grating with OAM-carrying far-field photons so that the angular momentum of the light (up to the polarization angular momentum) is imprinted onto the grating.

DISCUSSION

In summary, we have shown that polaritons with angular momentum allow for access to and control over absorption processes as a result of both conservation of angular momentum and extreme subwavelength confinement. This holds most readily when the absorbing atom is aligned with the vortex center. Nevertheless, control over electronic transitions (including non-angular-momentum-conserving ones) can even be obtained when atoms are randomly distributed in the vortex through two tuning parameters: polariton dispersion and distribution size. Due to the nanoscopic volumes and scales assumed in this work, we expect this method to be of greatest relevance to controlled experiments involving few emitters, as exemplified by recent studies.[56] The conclusions we arrive at hold for a wide range of polaritonic materials, whether they be plasmon, phonon, exciton, or other classes of polaritons.

Finally, we discuss interesting effects of light–matter interactions with vortex polaritons beyond single-photon processes. In the SI, we extend our formalism to consider the case where the atom absorbs two quanta of light, as would be the case in multiphoton spectroscopy. We find that when an atom (concentric with vortices) absorbs two vortex modes, the angular momentum selection rule becomes $m_f - m_i = m_{vortex,1} + m_{vortex,2}$, where $\hbar(m_f - m_i)$ is the change in z-projected orbital angular momentum of the electron and $\hbar m_{vortex,1}$, $\hbar m_{vortex,2}$ are the angular momenta of the two absorbed vortices. Therefore, it should be possible to tailor the selection rules of multiphoton spectroscopy through the use of two vortices with potentially different angular momenta. We find that the multiphoton interaction is strong for highly confined vortex modes.

In addition to absorption, we also considered spontaneous emission of vortex modes by an atom in order to pave the way for doing near-field quantum optics with vortex modes. We find that for emitters interfaced with polaritonic materials sustaining highly confined modes the spontaneous emission into one vortex (with high OAM) and into two vortices (with OAM 0 or $\pm\hbar$) can be quite fast. However, one would need an emitter with a highly m-dependent energy spectrum such that the decay rate of the emitter depends sharply on the OAM of the emitted polariton. In such a circumstance, one could have an emitter that selectively generates a single vortex quantum with a desired value of OAM or even potentially entangled vortex quanta.

In the long term, the ability to engineer the electronic transitions in a quantum system, enabled by polaritonic modes, opens the door for many applications that depend on usually inaccessible quantum states. Generating these quantum states in simple table-top settings will lead to novel light-emitting devices and even lasing technologies, by enabling new decay paths in quantum systems. At the same time, including OAM-carrying polariton modes in the toolbox of spectroscopy adds a new technique with which to probe and investigate electronic transitions and states, in particular in multielectron systems, where the large degeneracy of the states is lifted and an even greater control over the electronic transitions is allowed. In another direction, exploring stronger fields in OAM-carrying polaritons will give us access to regimes of nonperturbative physics, where the electronic states themselves are being altered. More generally, we believe this technique holds promising prospects for using the complete set of degrees of freedom in the temporal and spatial shaping of optical fields, for coherent control and engineering of the electron dynamics in quantum systems.

METHODS

We analyze the light–matter interaction by writing down the electromagnetic field operator in the basis of vortex modes and then using the resulting interaction Hamiltonian to compute the rates of various interaction processes between light and matter using Fermi's golden rule. The Hamiltonian and corresponding field operators are given below as

DOI: 10.1021/acsphotonics.8b00325
ACS Photonics 2018, 5, 3064–3072

$$H = H_{ele} + H_{SP(h)P} + H_{int} \text{ with}$$

$$H_{int} = \frac{e}{2m_e}(\boldsymbol{A}\cdot\boldsymbol{p} + \boldsymbol{p}\cdot\boldsymbol{A}) + \frac{e^2}{2m_e}\boldsymbol{A}^2 \text{ where}$$

$$\boldsymbol{A} = \sum_{q,m}\sqrt{\frac{\hbar q^2}{4\bar{\epsilon}_r\epsilon_0\omega_q L\xi_q}}(\boldsymbol{F}_{q,m}\hat{a}_{q,m} + \boldsymbol{F}^*_{q,m}\hat{a}^\dagger_{q,m}) \quad (4)$$

where H_{ele} is the Hamiltonian of the electron, $H_{SP(h)P}$ is the Hamiltonian of the SP(h)P modes, and H_{int} is the interaction Hamiltonian between the electron and SP(h)Ps. m_e and e are the mass and charge of the electron, ϵ_0 the vacuum permittivity, $\bar{\epsilon}_r$ the average relative permittivity of the dielectric above and below the interface, and L the quantization length of the system. $\boldsymbol{A}$ corresponds to the vector potential operator and it is written as an expansion over dimensionless modes of the vector potential $\boldsymbol{F}_{q,m}$, with corresponding creation (annihilation) operators $\hat{a}^\dagger_{q,m}$ ($\hat{a}_{q,m}$). These modes can be derived from the integral expression in eq 1:

$$\boldsymbol{F}_{q,m} = e^{-q|z|}\frac{1}{2\sqrt{2}}e^{im\phi}i^{m+1}\left\{\hat{\rho}[J_{m+1}(q\rho) - J_{m-1}(q\rho)] - i\hat{\phi}\frac{2mJ_m(q\rho)}{q\rho} + \begin{Bmatrix}\hat{z}2J_m(q\rho) & (z>0)\\ 0 & (z=0)\\ -\hat{z}2J_m(q\rho) & (z<0)\end{Bmatrix}\right\} \quad (5)$$

where $J_m(q\rho)$ is the Bessel function of order m, ρ, ϕ, and z are the standard cylindrical coordinates, and q is the wavenumber of the mode. The parameter ξ_q is a dimensionless normalization factor that is required for the energy of the vortex mode to be $\hbar\omega$. We find that the factor $\xi_q v_g$, where $v_g = d\omega/dq$ is the group velocity, dictates the strength of light−matter interactions and is similar for polaritons in different materials with the same confinement factor. The details of our calculations are provided in the SI.

■ ASSOCIATED CONTENT

Supporting Information

The Supporting Information is available free of charge on the ACS Publications website at DOI: 10.1021/acsphotonics.8b00325.

Analysis of transition rates for a different set of hydrogenic transitions. Second quantization of polaritons in the orbital angular momentum basis and in different gauges. Calculation of transition amplitudes for absorption and emission of a polariton with orbital angular momentum at first and second order in perturbation theory (PDF)

■ AUTHOR INFORMATION

Corresponding Author

*E-mail: fmachado@berkeley.edu.

ORCID

Francisco Machado: 0000-0003-0068-5073

Nicholas Rivera: 0000-0002-8298-1468

Author Contributions

⊥F.M. and N.R. are equal-contributing first authors. F.M., N.R., and I.K. conceived the idea. F.M. and N.R. performed the analytical and numerical calculations. H.B., M.S., and I.K. supervised the research. All authors contributed to the manuscript preparation and revision.

Notes

The authors declare no competing financial interest.

■ ACKNOWLEDGMENTS

This work was partially motivated by discussions with Moti Segev on whether the orbital angular momentum of light is an intrinsic property of the single photon or a joint property of the ensemble of photons. Research was supported as part of the Army Research Office through the Institute for Soldier Nanotechnologies under contract no. W911NF-13-D-0001 (photon management for developing nuclear-TPV and fuel-TPV mm-scale-systems) and supported as part of the S3TEC, an Energy Frontier Research Center funded by the U.S. Department of Energy under grant no. DE-SC0001299 (for fundamental photon transport related to solar TPVs and solar-TEs). N.R. was supported by a Department of Energy fellowship no. DE-FG02-97ER25308. H.B. acknowledges support from the QuantiXLie Center of Excellence. I.K. is an Azrieli Fellow, supported by the Azrieli Foundation, and was partially supported by the Seventh Framework Programme of the European Research Council (FP7-Marie Curie IOF) under grant no. 328853-MC-BSiCS.

■ REFERENCES

(1) Allen, L.; Beijersbergen, M. W.; Spreeuw, R. J. C.; Woerdman, J. P. Orbital angular momentum of light and the transformation of Laguerre-Gaussian laser modes. *Phys. Rev. A: At., Mol., Opt. Phys.* **1992**, *45*, 8185−8189.

(2) He, H.; Friese, M.; Heckenberg, N.; Rubinsztein-Dunlop, H. Direct observation of transfer of angular momentum to absorptive particles from a laser beam with a phase singularity. *Phys. Rev. Lett.* **1995**, *75*, 826−829.

(3) Lavery, M. P. J.; Speirits, F. C.; Barnett, S. M.; Padgett, M. J. Detection of a spinning object using light's orbital angular momentum. *Science (Washington, DC, U. S.)* **2013**, *341*, 537−40.

(4) Yan, Y.; Xie, G.; Lavery, M. P. J.; Huang, H.; Ahmed, N.; Bao, C.; Ren, Y.; Cao, Y.; Li, L.; Zhao, Z.; Molisch, A. F.; Tur, M.; Padgett, M. J.; Willner, A. E. High-capacity millimetre-wave communications with orbital angular momentum multiplexing. *Nat. Commun.* **2014**, *5*, 4876.

(5) Wang, J.; Yang, J.-Y.; Fazal, I. M.; Ahmed, N.; Yan, Y.; Huang, H.; Ren, Y.; Yue, Y.; Dolinar, S.; Tur, M.; Willner, A. E. Terabit free-space data transmission employing orbital angular momentum multiplexing. *Nat. Photonics* **2012**, *6*, 488−496.

(6) Ren, H.; Li, X.; Zhang, Q.; Gu, M. On-chip noninterference angular momentum multiplexing of broadband light. *Science (Washington, DC, U. S.)* **2016**, *352*, 805−809.

(7) Molina-Terriza, G.; Torres, J. P.; Torner, L. Twisted photons. *Nat. Phys.* **2007**, *3*, 305−310.

(8) Nicolas, A.; Veissier, L.; Giner, L.; Giacobino, E.; Maxein, D.; Laurat, J. A quantum memory for orbital angular momentum photonic qubits. *Nat. Photonics* **2014**, *8*, 234−238.

(9) Mair, A.; Vaziri, A.; Weihs, G.; Zeilinger, A. Entanglement of the orbital angular momentum states of photons. *Nature* **2001**, *412*, 313−6.

(10) Mirhosseini, M.; Magaña-Loaiza, O. S.; O'Sullivan, M. N.; Rodenburg, B.; Malik, M.; Lavery, M. P. J.; Padgett, M. J.; Gauthier, D. J.; Boyd, R. W. High-dimensional quantum cryptography with twisted light. *New J. Phys.* **2015**, *17*, 033033.

(11) Malik, M.; Erhard, M.; Huber, M.; Krenn, M.; Fickler, R.; Zeilinger, A. Multi-photon entanglement in high dimensions. *Nat. Photonics* **2016**, *10*, 248−252.

(12) Yao, A. M.; Padgett, M. J. Orbital angular momentum: origins, behavior and applications. *Adv. Opt. Photonics* **2011**, *3*, 161.

DOI: 10.1021/acsphotonics.8b00325
ACS Photonics 2018, 5, 3064−3072

(13) Picón, A.; Benseny, A.; Mompart, J.; Vázquez de Aldana, J. R.; Plaja, L.; Calvo, G. F.; Roso, L. Transferring orbital and spin angular momenta of light to atoms. *New J. Phys.* **2010**, *12*, 083053.
(14) Picón, A.; Mompart, J.; de Aldana, J. R. V.; Plaja, L.; Calvo, G. F.; Roso, L. Photoionization with orbital angular momentum beams. *Opt. Express* **2010**, *18*, 3660−71.
(15) Afanasev, A.; Carlson, C. E.; Mukherjee, A. Off-axis excitation of hydrogenlike atoms by twisted photons. *Phys. Rev. A: At., Mol., Opt. Phys.* **2013**, *88*, 033841.
(16) Afanasev, A.; Carlson, C. E.; Mukherjee, A. High-multipole excitations of hydrogen-like atoms by twisted photons near a phase singularity. *J. Opt.* **2016**, *18*, 074013.
(17) Asenjo-Garcia, A.; de Abajo, F. G. Dichroism in the interaction between vortex electron beams, plasmons, and molecules. *Phys. Rev. Lett.* **2014**, *113*, 066102.
(18) Schmiegelow, C. T.; Schulz, J.; Kaufmann, H.; Ruster, T.; Poschinger, U. G.; Schmidt-Kaler, F. Transfer of optical orbital angular momentum to a bound electron. *Nat. Commun.* **2016**, *7*, 12998.
(19) Jablan, M.; Buljan, H.; Soljačić, M. Plasmonics in graphene at infrared frequencies. *Phys. Rev. B: Condens. Matter Mater. Phys.* **2009**, *80*, 245435.
(20) Ju, L.; Geng, B.; Horng, J.; Girit, C.; Martin, M.; Hao, Z.; Bechtel, H. A.; Liang, X.; Zettl, A.; Shen, Y. R.; Wang, F. Graphene plasmonics for tunable terahertz metamaterials. *Nat. Nanotechnol.* **2011**, *6*, 630−634.
(21) Chen, J.; Badioli, M.; Alonso-González, P.; Thongrattanasiri, S.; Huth, F.; Osmond, J.; Spasenović, M.; Centeno, A.; Pesquera, A.; Godignon, P.; Elorza, A. Z.; Camara, N.; García de Abajo, F. J.; Hillenbrand, R.; Koppens, F. H. L. Optical nano-imaging of gate-tunable graphene plasmons. *Nature* **2012**, *487*, 77−81.
(22) Grigorenko, A. N.; Polini, M.; Novoselov, K. S. Graphene plasmonics. *Nat. Photonics* **2012**, *6*, 749−758.
(23) Caldwell, J. D.; Lindsay, L.; Giannini, V.; Vurgaftman, I.; Reinecke, T. L.; Maier, S. A.; Glembocki, O. J. Low-loss, infrared and terahertz nanophotonics using surface phonon polaritons. *Nanophotonics* **2015**, *4*, 44−68.
(24) Hillenbrand, R.; Taubner, T.; Keilmann, F. Phonon-enhanced light matter interaction at the nanometre scale. *Nature* **2002**, *418*, 159−62.
(25) Greffet, J.-J.; Carminati, R.; Joulain, K.; Mulet, J.-P.; Mainguy, S.; Chen, Y. Coherent emission of light by thermal sources. *Nature* **2002**, *416*, 61−64.
(26) Liu, Y.; Willis, R. F.; Emtsev, K. V.; Seyller, T. Plasmon dispersion and damping in electrically isolated two-dimensional charge sheets. *Phys. Rev. B: Condens. Matter Mater. Phys.* **2008**, *78*, 201403.
(27) Fei, Z.; Andreev, G. O.; Bao, W.; Zhang, L. M.; McLeod, A. S.; Wang, C.; Stewart, M. K.; Zhao, Z.; Dominguez, G.; Thiemens, M.; Fogler, M. M.; Tauber, M. J.; Castro-Neto, A. H.; Lau, C. N.; Keilmann, F.; Basov, D. N. Infrared nanoscopy of dirac plasmons at the graphene-SiO$_2$ interface. *Nano Lett.* **2011**, *11*, 4701−5.
(28) Fei, Z.; Rodin, A. S.; Andreev, G. O.; Bao, W.; McLeod, A. S.; Wagner, M.; Zhang, L. M.; Zhao, Z.; Thiemens, M.; Dominguez, G.; Fogler, M. M.; Castro Neto, A. H.; Lau, C. N.; Keilmann, F.; Basov, D. N. Gate-tuning of graphene plasmons revealed by infrared nano-imaging. *Nature* **2012**, *487*, 82−5.
(29) Nagao, T.; Hildebrandt, T.; Henzler, M.; Hasegawa, S. Dispersion and damping of a two-dimensional plasmon in a metallic surface-state band. *Phys. Rev. Lett.* **2001**, *86*, 5747−50.
(30) Diaconescu, B.; Pohl, K.; Vattuone, L.; Savio, L.; Hofmann, P.; Silkin, V. M.; Pitarke, J. M.; Chulkov, E. V.; Echenique, P. M.; Farías, D.; Rocca, M. Low-energy acoustic plasmons at metal surfaces. *Nature* **2007**, *448*, 57−9.
(31) Caldwell, J. D.; Glembocki, O. J.; Francescato, Y.; Sharac, N.; Giannini, V.; Bezares, F. J.; Long, J. P.; Owrutsky, J. C.; Vurgaftman, I.; Tischler, J. G.; Wheeler, V. D.; Bassim, N. D.; Shirey, L. M.; Kasica, R.; Maier, S. A. Low-loss, extreme subdiffraction photon confinement via silicon carbide localized surface phonon polariton resonators. *Nano Lett.* **2013**, *13*, 3690−7.
(32) Caldwell, J. D.; Kretinin, A. V.; Chen, Y.; Giannini, V.; Fogler, M. M.; Francescato, Y.; Ellis, C. T.; Tischler, J. G.; Woods, C. R.; Giles, A. J.; Hong, M.; Watanabe, K.; Taniguchi, T.; Maier, S. A.; Novoselov, K. S. Sub-diffractional volume-confined polaritons in the natural hyperbolic material hexagonal boron nitride. *Nat. Commun.* **2014**, *5*, 5221.
(33) Woessner, A.; Lundeberg, M. B.; Gao, Y.; Principi, A.; Alonso-González, P.; Carrega, M.; Watanabe, K.; Taniguchi, T.; Vignale, G.; Polini, M.; Hone, J.; Hillenbrand, R.; Koppens, F. H. L. Highly confined low-loss plasmons in graphene-boron nitride heterostructures. *Nat. Mater.* **2015**, *14*, 421−5.
(34) Tomadin, A.; Principi, A.; Song, J. C. W.; Levitov, L. S.; Polini, M. Accessing Phonon Polaritons in Hyperbolic Crystals by Angle-Resolved Photoemission Spectroscopy. *Phys. Rev. Lett.* **2015**, *115*, 087401.
(35) Bondarev, I.; Lambin, P. Spontaneous-decay dynamics in atomically doped carbon nanotubes. *Phys. Rev. B: Condens. Matter Mater. Phys.* **2004**, *70*, 035407.
(36) Koppens, F. H.; Chang, D. E.; Garcia de Abajo, F. J. Graphene plasmonics: a platform for strong light-matter interactions. *Nano Lett.* **2011**, *11*, 3370−3377.
(37) Zurita-Sánchez, J. R.; Novotny, L. Multipolar interband absorption in a semiconductor quantum dot. I. Electric quadrupole enhancement. *J. Opt. Soc. Am. B* **2002**, *19*, 1355−1362.
(38) Zurita-Sánchez, J. R.; Novotny, L. Multipolar interband absorption in a semiconductor quantum dot. II. Magnetic dipole enhancement. *J. Opt. Soc. Am. B* **2002**, *19*, 2722−2726.
(39) Filter, R.; Mühlig, S.; Eichelkraut, T.; Rockstuhl, C.; Lederer, F. Controlling the dynamics of quantum mechanical systems sustaining dipole-forbidden transitions via optical nanoantennas. *Phys. Rev. B: Condens. Matter Mater. Phys.* **2012**, *86*, 035404.
(40) Jain, P. K.; Ghosh, D.; Baer, R.; Rabani, E.; Alivisatos, A. P. Near-field manipulation of spectroscopic selection rules on the nanoscale. *Proc. Natl. Acad. Sci. U. S. A.* **2012**, *109*, 8016−8019.
(41) Alabastri, A.; Yang, X.; Manjavacas, A.; Everitt, H. O.; Nordlander, P. Extraordinary light-induced local angular momentum near metallic nanoparticles. *ACS Nano* **2016**, *10*, 4835−4846.
(42) Takase, M.; Ajiki, H.; Mizumoto, Y.; Komeda, K.; Nara, M.; Nabika, H.; Yasuda, S.; Ishihara, H.; Murakoshi, K. Selection-rule breakdown in plasmon-induced electronic excitation of an isolated single-walled carbon nanotube. *Nat. Photonics* **2013**, *7*, 550−554.
(43) Yannopapas, V.; Paspalakis, E. Giant enhancement of dipole-forbidden transitions via lattices of plasmonic nanoparticles. *J. Mod. Opt.* **2015**, *62*, 1435−1441.
(44) Andersen, M. L.; Stobbe, S.; Sørensen, A. S.; Lodahl, P. Strongly modified plasmonmatter interaction with mesoscopic quantum emitters. *Nat. Phys.* **2011**, *7*, 215−218.
(45) Rukhlenko, I. D.; Handapangoda, D.; Premaratne, M.; Fedorov, A. V.; Baranov, A. V.; Jagadish, C. Spontaneous emission of guided polaritons by quantum dot coupled to metallic nanowire: Beyond the dipole approximation. *Opt. Express* **2009**, *17*, 17570−17581.
(46) Kurman, Y.; Rivera, N.; Christensen, T.; Tsesses, S.; Orenstein, M.; Soljačić, M.; Joannopoulos, J. D.; Kaminer, I. Control of semiconductor emitter frequency by increasing polariton momenta. *Nat. Photonics* **2018**, *12*, 423−429.
(47) Rivera, N.; Kaminer, I.; Zhen, B.; Joannopoulos, J. D.; Soljačić, M. Shrinking light to allow forbidden transitions on the atomic scale. *Science (Washington, DC, U. S.)* **2016**, *353*, 263−9.
(48) Rivera, N.; Rosolen, G.; Joannopoulos, J. D.; Kaminer, I.; Soljačić, M. Making two-photon processes dominate one-photon processes using mid-IR phonon polaritons. *Proc. Natl. Acad. Sci. U. S. A.* **2017**, *114*, 13607−13612.
(49) David, A.; Gjonaj, B.; Blau, Y.; Dolev, S.; Bartal, G. Nanoscale shaping and focusing of visible light in planar metaloxidesilicon waveguides. *Optica* **2015**, *2*, 1045.
(50) Spektor, G.; David, A.; Gjonaj, B.; Bartal, G.; Orenstein, M. Metafocusing by a Metaspiral Plasmonic Lens. *Nano Lett.* **2015**, *15*, 5739−43.
(51) David, A.; Gjonaj, B.; Bartal, G. Two-dimensional optical nanovortices at visible light. *Phys. Rev. B: Condens. Matter Mater. Phys.* **2016**, *93*, 121302.

DOI: 10.1021/acsphotonics.8b00325
ACS Photonics 2018, 5, 3064−3072

(52) Spektor, G.; Kilbane, D.; Mahro, A. K.; Frank, B.; Ristok, S.; Gal, L.; Kahl, P.; Podbiel, D.; Mathias, S.; Giessen, H.; Meyer zu Heringdorf, F.-J.; Orenstein, M.; Aeschlimann, M. Revealing the subfemtosecond dynamics of orbital angular momentum in nanoplasmonic vortices. *Science* **2017**, *355*, 1187−1191.
(53) Chang, C.-H.; Rivera, N.; Joannopoulos, J. D.; Soljačić, M.; Kaminer, I. Constructing "Designer Atoms" via Resonant Graphene-Induced Lamb Shifts. *ACS Photonics* **2017**, *4*, 3098−3105.
(54) Andersen, M. L.; Stobbe, S.; Sørensen, A. S.; Lodahl, P. Strongly modified plasmon-matter interaction with mesoscopic quantum emitters. *Nat. Phys.* **2011**, *7*, 215−218.
(55) Scholz-Marggraf, H. M.; Fritzsche, S.; Serbo, V. G.; Afanasev, A.; Surzhykov, A. Absorption of twisted light by hydrogenlike atoms. *Phys. Rev. A: At., Mol., Opt. Phys.* **2014**, *90*, 013425.
(56) Chikkaraddy, R.; de Nijs, B.; Benz, F.; Barrow, S. J.; Scherman, O. A.; Rosta, E.; Demetriadou, A.; Fox, P.; Hess, O.; Baumberg, J. J. Single-molecule strong coupling at room temperature in plasmonic nanocavities. *Nature* **2016**, *535*, 127.

DOI: 10.1021/acsphotonics.8b00325
ACS Photonics 2018, 5, 3064−3072